Dynamic Road Surface Detection Method based on 3D Lidar

Yi-Shueh Tsai
Applied Sensor Technology Group, R&D department
Automotive Research and Testing Center (ARTC)
Changhua County, TAIWAN (R.O.C)
jefftsai@artc.org.tw

Yu-Fang Wang
Applied Sensor Technology Group, R&D department
Automotive Research and Testing Center (ARTC)
Changhua County, TAIWAN (R.O.C)
ashley@artc.org.tw

***Abstract*—This paper propose a road surface classification method based on 3D-lidar that is not required to be high-resolution. Lidar range data is transformed with static calibration result, and the near-ground points are extracted with a ground elevation estimation method. After filling the scanning gaps with interpolation, the continuity of each scan lines at each point is examined by its polar interpretation. The smoothness is analyzed in the same interpretation with simple linear regression to evaluate the estimated angle feature. The road boundaries defined by the two criteria form the road surface with region growing method. The proposed method has been verified through actual road scenario to show its robustness and efficiency on two different vehicle mounting configurations.**

Keywords—lidar; road; ground; growing; classification

I. INTRODUCTION

In autonomous driving sensing, it is important to build reliable perception of surrounding environment, and conduct precise detection of objects and free road space. Among many proposed approaches satisfying the requirements above, the use of lidar sensor has been proven reliable for its high resolution and precision. With high-frequency laser pulse emission-reception, lidar measures the distance between the sensor and the target points. A 3D lidar combine a rotational device with laser modules to obtain a 3D depth map within its vertical field of view. In the 3D lidar-scanned depth map analysis, ground point classification is a crucial step, as its precision impacts the quality of all following steps. In urban road environment, the ground classification consist of detecting road and road-edge, in order to detect area available for passing and distinguish from the ground the objects and road infrastructures that has to be avoided.

Many studies achieve road and road-edge detection using high definition 3D lidar such as Velodyne HDL-64 High Definition Lidar [1], where the generated point cloud data is enough dense and nearly isotropic (approximately 1 : 2.5 horizontal-vertical resolution ratio, with horizontal resolution 0.16 degrees at 10 Hz rotation, vertical resolution $\simeq$ 0.4 degrees) to be analyzed assuming the point cloud distribution is almost isotropic, e.g. mesh-based point cloud analysis combined with local convexity segmentation [2]. Other research may benefits from planar detection of 2D lidar to detect road and road-edge, e.g. [3]. To deal with high density point clouds, some studies produce grid map with 3D points using MKV model and LBF algorithm to extracting the feature of road like [4] and [5].

In the case of lower definition 3D lidar scanner such as Velodyne VLP-16 lidar, its approximate 10:1 horizontal-vertical resolution ratio makes mesh grids triangles vertically slender. Plus, the fact that vertically consecutive points (whose corresponding laser pulses are vertically separated by 2° in the case of Velodyne VLP-16) are very likely to belong to completely distinct surfaces and different objects, which often makes the distance comparison between them inconclusive and meaningless. In consequence, mesh-based methods are less applicable to the point cloud generated by low resolution lidar.

Compared to 2D lidar, multiple scan layers of 3D lidar produce much richer information. However, these layers are non-planar and have distinct angle of incline, which makes their detection pattern different from one scan layer to another. Plus, as the planar assumption become invalid, ground detection methods used in 2D lidar [6] does not apply to individual scan layer. Another distinction is that 2D lidar based ground detection aim to accumulate scan results over time as the mounted scanner geographically moves with the vehicle on which it is mounted, in order to obtain ground area information. If the information can be obtained within a single spin of a 3D lidar and keep the information updated upon each scanning frame, the provided perception will be more instantaneous and secure, and thus more compatible to automated driving scenario requirements.

To build perception of road based on sensors mounted on a vehicle driving on actual road, there are several factors to be taken into account, notably the pitch and roll angles variation in vehicle movement, sloped, rugged and curved road surface, different sensor mounting angle / position, and different kinds and direction of road edge.

The vibration and dynamic position change of a moving vehicle causes the height and angle of the mounted sensor to vary. Such variation becomes more significant when an intense acceleration or braking takes place, where the sensor pitched respectively upward and downward.

Most road surface is not a perfect plane. Most road are designed to have 1~2 degree cross slope to enable water drainage. Likewise, Climbing sloped road surface may also appear elevated, but it should not be considered as an object or

a road edge. Other factors such as road hump and manhole cover can also make road surface uneven, e.g.[7]. Other methods to build road surface also includes using deep learning approach to train the feature of point cloud, e.g. [8].

As the lidar sensor can be applied on various applications, it may be mounted on different positions with different mounting angles. Two common choices are mounted horizontally on top of the vehicle for around-view detection, and mounted in front of the vehicle slightly pitched down to optimize forward detection (see Figure 1). It's clear that different mounting position and angle will produce different scanning pattern even with identical sensor, so it is important to make the detection method to adapt to different mounting positions and angles.

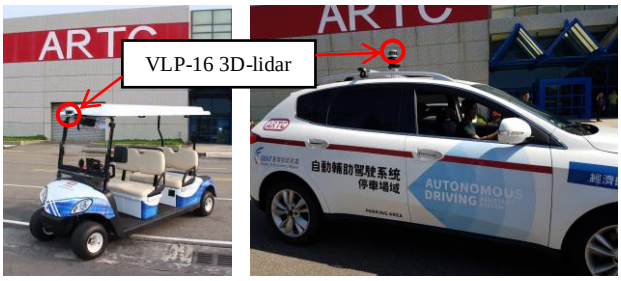

Figure 1. Illustration two 3D lidar mounting configuration: (Left) 3D lidar mounted in front of a golf-car. (Right) 3D lidar mounted on the top of an SUV.

Although road edges are usually a vertical surface, but an amount of variation can be found on actual road, non-vertical curb, fence, grass ...etc. The road edges may appear facing many different possible directions, which further pose challenge to road edge detection.

The purpose of this work is to develop a robust road surface and road edge detection technique based on only a single low-resolution 3D lidar such as Velodyne VLP-16 lidar. The proposed method aims to solve the above-mentioned problems.

II. Road and Road-Edge Detection

A. Overview

A cascade processing method is proposed to detect road and road-edge, composed of the following steps as shown in Figure 2: depth data acquisition, static calibration, reference slope calculation, elevated point removal, scan line smoothness [9] & height analysis, feature point extraction, road-edge reconstruction, and road area acquisition.

The lidar scan data is first received, stored and processed frame by frame. The acquired scan data is then transformed based on static calibration results. A reference slope is then calculated with an elevation affine ladder estimation method, which is more efficient than the RANSAC-based method used applied in [6] and [10]. With this reference slope, points that are too elevated can be removed to reduce unnecessary processing. The remainders are processed with continuity, smoothness and height criterion to locate road boundary feature points. By reconstructing road-edge surfaces with region growing method, road perception can be built.

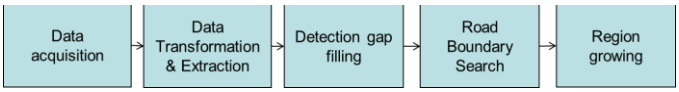

Figure 2. Flow chart of road detection algorithm

B. Data acquisition

The data scanned by VLP-16 is transmitted through an Ethernet cable to the reception device, which in our case is a laptop. In 10 Hz rotation, each spin of lidar takes 0.1 second and generates ≈ 28,000 scan points of surrounding environment with progressively increasing azimuth angle. Yet there will be a 0.1 second detection time discontinuity gap across the end and beginning of the scan. For autonomous driving application, front scanning is considered the most important, so it is wise to choose the rear of the scanning to be the boundary of a frame.

C. Coordinate transformation & static calibration

The data scanned by VLP-16 correspond to position relative to the sensor. It has to be transformed to vehicle coordinate system for later applications. The necessary parameters such as mounting position of lidar (x_0, y_0, h), mounting pitch angle α, roll angle β (see Figure 3) are obtained by static calibration: measure the relative position and mounting angle of the sensor with the vehicle where it is mounted on parked stably on a flat ground. Let (x', y', z') be the coordinate of the scan point in the relative coordinate system as observed by lidar, and (x, y, z) the coordinate in vehicle coordinate system (see Figure 3). We have the below translate equation:

$$\begin{bmatrix} x \\ y \\ z \end{bmatrix} = \begin{bmatrix} x_0 \\ y_0 \\ h \end{bmatrix} + \begin{bmatrix} \cos\beta & 0 & \sin\beta \\ 0 & 1 & 0 \\ -\sin\beta & 0 & \cos\beta \end{bmatrix} \times \begin{bmatrix} 1 & 0 & 0 \\ 0 & \cos\alpha & \sin\alpha \\ 0 & -\sin\alpha & \cos\alpha \end{bmatrix} \times \begin{bmatrix} x' \\ y' \\ z' \end{bmatrix} \quad (1)$$

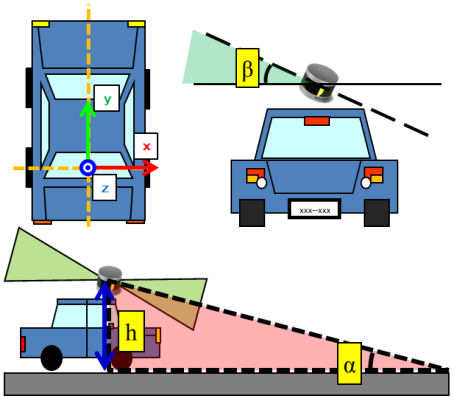

Figure 3. (Top left) Vehicle coordinate system centered at middle of the rear wheel axis (Top right) Illustration of mounting roll angle β (Bottom) Illustration of mounting height h and mounting pitch angle α

D. Reference slope estimation

Although the static calibration mentioned above has been done, during the vehicle movement, the height and angle variation as well as the presence of the road slope has to be taken into account. For each scanning frame, we sample points whose projection on x-y plane located in a rectangle area of 16 m (width, x-direction) × 20 m (length, y-direction) in front of the vehicle, and we decompose it into 16 m x 1 m blocks. For each block, if the number of points presents is above a threshold n, we find the minimal height of points within the block; if not, we find the minimal height with the interpolation

of the previous and the next area height. If a slope of 30% is present across two valid blocks, which may mean the presence of large objects that either locates near the block or shades the detection points, we replace the block height with interpolated value. This way, we obtain a height and distance correspondence curve (z-y relation) with 1 m horizontal resolution. This curve will be considered as the reference ground for the following processing steps, where the height corresponding to a random distance in front of the vehicle can be calculated with the table with interpolation. (see Figure 4)

E. Elevated point removal

As the referenced slope is obtained, we can remove the points located above a certain height H. Scan points corresponding to tall objects and buildings are removed from scan data as they are too far away from possible ground surface.

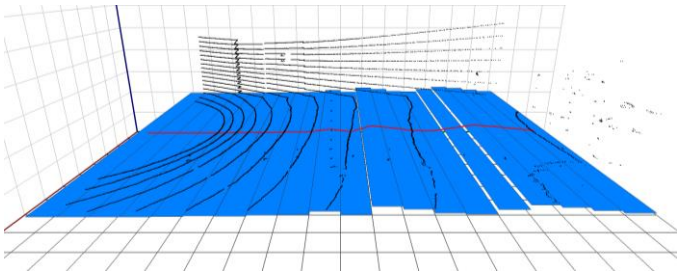

Figure 4. Illustration results of slope estimation, the height estimation curve is plotted on the y-z plane in red, each 2m × 1m rectangle are plotted in blue, and the points located above the 2m × 20m area are plotted in black. The scale of z-direction is magnified 10 times to make variation more visible. Data set recorded from lidar mounted on a golf-car with a static downward pitch angle (Top) Vehicle pitched to ground (Bottom) Vehicle pitched upward.

F. Detection gap filling

Within each scan layer, detection loss (where a laser firing returns no response) was found on multiple testing scenarios. The loss may occur even on ordinary road surface within 15m, and is observed to occur much more recently on the painted area on the road, including lane marks and road signs. Since we wish to conserve the regularity of azimuth increment along the scan, it is wise to apply a "gap filling" interpolation technique: apply an affine interpolation to a pair of nun-null points that satisfies following conditions:

(a)All points between the two points are null returns.

(b)The two terminal points fulfill the proximity criteria: $dist(point1, point2) < \gamma$

(c)The number of null points between two terminal points does not exceed a tolerance level L_{tol}

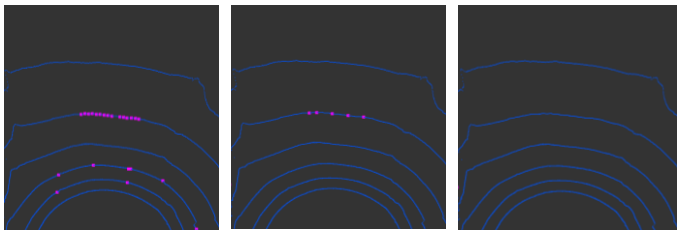

Figure 5. Top-down view of detection gap filling at road intersection entry scenario, consecutive points are marked in blue, the terminal points of null return are highlighted in magenta. Results are generated with respective L_{tol} = 0 (left), L_{tol} = 1 (center) and L_{tol} = 2 (right)

G. Scan line continuity filter

To detect road area, we have to determine the border of the road, which may be present in various forms, including obstacles on the road and the road curb on both side of the road. The previous is characterized with the discontinuity of scan line, and the later are characterized with the rapid angle change on continuous scan lines.

A point in the lidar relative coordination system can be described in polar coordinate representation $P(R, \theta, \varphi)$, where θ is azimuth and φ is vertical angle of the point. A scan line, where the vertical angle φ is constant by the design of rotational lidar such as Velodyne VLP-16 lidar, can be represented as below:

$$\{ P(\theta) = (R(\theta), \theta, \varphi = const), \theta = 0°..360° \}$$

The presentation shows the continuity of the scan line in the space can be characterized with the continuity of the function $R(\theta)$. Since points are detected with equal azimuth intervals (for VLP-16 lidar scanning with 10Hz, each interval = 0.16°), we can consider the returned distance sequence $(R_i, i = 1 \cdots n)$, as a regular sampling of $R(\theta)$, thus the discontinuity of can be further modelized as a value leap of the distance sequence as below :

$$(P(t), 0° \le t < 360°) is\ discontinue\ on\ \theta$$
$$\Leftrightarrow \frac{R(\theta + \delta) - R(\theta)}{\delta} \underset{\delta \to 0}{\longrightarrow} \infty$$
$$\underset{sampling}{\Longleftrightarrow} |R_i - R_{i-1}| \ge \varepsilon_c \& |R_{i+1} - R_i| \ge \varepsilon_c$$

Thus our continuity criterion is obtained as below:

$$\max(|R_i - R_{i-1}|, |R_i - R_{i+1}|) < \varepsilon_c \qquad (2)$$

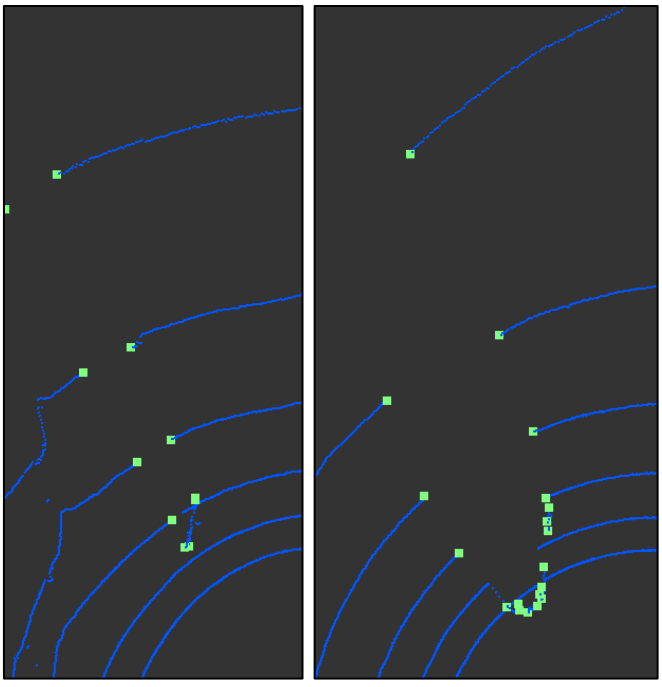

Figure 6. The continuity filter applied on test scene with the presence of objects, the continuous points are marked in blue, and the discontinuous points are marked in light green. (left) the scene with the presence of a motorcycle (right) the scene with the presence of a vehicle, where the road-object boundary in second nearest scan line was not detected by the continuity filter

The above Figure 6 Shows the edge of object as well as the terminal of obstructed scan lines are marked with the applied continuity filter. Some exception appears at the bottom of the object that touches the ground continuously or with a very small gap. Although such case cannot be detected using the continuity filter, the smoothness filter in the next paragraph will be able to distinguish the transition point between ground and object. We can also observe that the ground detection area obstructed by the object is not limited to the ground beneath the object, but also a "shade" area that, depending on the height of object, may extends to more than 20m.

H. Scan line smoothness filter

Traditional smoothness analysis evaluates double differentiation $\frac{d^2R}{(d\theta)^2}$ peak values to find point with angle transition. We require in our case a noise-resisting filter that can find transitions in a larger scope to adapt to detection noise and sequenced scan line.

Our goal is to find the presence of an angle on the point sequence in a scan-line in 3-dimension space. The angle is defined by the angle between "trend line" before and after the examined point. However, the random distribution of points and uncertain direction of angle plane make the angle in 3-dimension space harder to determine. Here we propose a space-to-plane transformation to approximate this angle.

Knowing that the beams of the same scan-layer with the same vertical angle φ < 15° will form a cone. We choose a number k of consecutive points inclusively before (in sense of point sequence with azimuth increment) the examined point $P_{\varphi,i}$. If k is chosen enough little (for instance k<10), the k consecutive points are approximately located on the tangent plane of the cone that passes through segment $\overline{OP_{\varphi,i}}$.

With same reason, the k consecutive points inclusively after $P_{\varphi,i}$ are located approximately on the same tangent plane passing through $\overline{OP_{\varphi,i}}$. We project all selected points and their central distance R and horizontal separation angle δ (δ=0.16 at 10Hz rotation), and obtain the first plane transformation as presented below in Figure 7. The angle in the space can be approximated by the angle between two trend line $\overline{P_{\varphi,i-k+1}\cdots P_{\varphi,i}}$ and $\overline{P_{\varphi,i}\cdots P_{\varphi,i+k-1}}$.

Knowing that k and δ are enough little, the radiation representation can be further transformed into an orthogonal representation. We remain on the same tangent plane, and place all points by order and separated by regular gap $R_i\delta$ while conserving their central distance to become R-direction coordinate(vertical distance in the plane). The representation is shown in Figure 7 below, and the angle is approximately conserved between the radiation representation and the orthogonal representation.

Back to the smoothness requirement, we can now approximately determine the 3-dimension angle by calculating the planar angle in the orthogonal representation. It remains only to obtain the slope of the trend line by simple linear regression method.

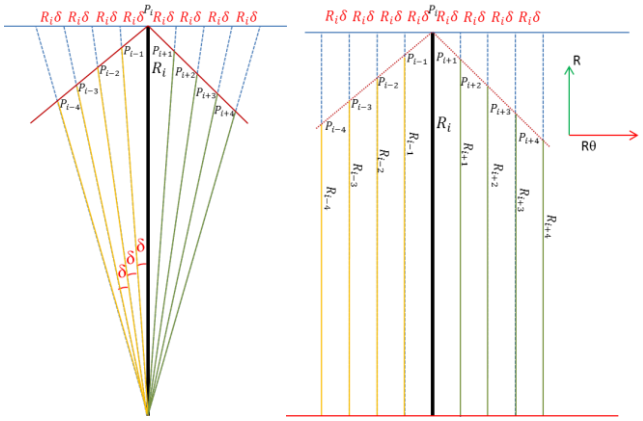

Figure 7. The two step angle approximation by transforming the 3-dimension distribution to radiation representation then to orthogonal representation

With regular horizontal gap$R_{i,\varphi}\cdot\delta$, the "before" trend line's slope can be obtained as below:

$$S_b = \frac{\sum_{j=1}^{k}\left(R_{i,\varphi}\cdot\theta_{\varphi,i-k+j} - R_{i,\varphi}\cdot\bar{\theta}\right)\cdot\left(R_{i-k+j} - \overline{R_{i-k+1..i,\varphi}}\right)}{\sum_{j=1}^{k}\left(R_{i,\varphi}\cdot\theta_{\varphi,i-k+j} - R_{i,\varphi}\cdot\bar{\theta}\right)^2}$$

$$= \frac{12\cdot\sum_{j=1}^{k}(j-\frac{k+1}{2})\cdot R_{i-k+j,\varphi}}{k(k-1)(k+1)\cdot R_{i,\varphi}\cdot\delta}$$

Same method can be applied to obtain the "after" trend line slope:

$$S_a = \frac{12\cdot\sum_{j=1}^{k}(j-\frac{k+1}{2})\cdot R_{i-1+j,\varphi}}{k(k-1)(k+1)\cdot R_{i,\varphi}\cdot\delta}$$

Let $\rho_c$be the angle between two lines, $\rho_b$the angle between "before" line and Rθ axis, and $\rho_a$the angle between "after" line and Rθ axis, we evaluate the tangent value of ρ_c

$$\tan\rho_c = \frac{\tan\rho_a - \tan\rho_b}{1+\tan\rho_a\cdot\tan\rho_b} = \frac{S_a - S_b}{1+S_a\cdot S_b} \quad (3)$$

This tangent value is chosen to be our corner point detection filter:

$$(\mathrm{P}(t), 0° \le t < 360°)\ has\ an\ angle\ on\ \theta$$
$$\Leftrightarrow \left|\frac{S_a - S_b}{1+S_a\cdot S_b}\right| = |tan\,\rho_c| \ge \varepsilon_s \quad (4)$$

Thus our smoothness criterion is obtained as below:

$$\left|\frac{S_a - S_b}{1+S_a\cdot S_b}\right| < \varepsilon_s \quad (5)$$

It can be observed that higher regression level N_{lr} (N_{lr}= k in previous formula) makes the filter less sensitive and more noise-resistant (as shown in Figure 8). Depending on the smoothness of the road and distance of the point, an adequate N_{lr} level is chosen to adapt different road surface smoothness and different detection scale.

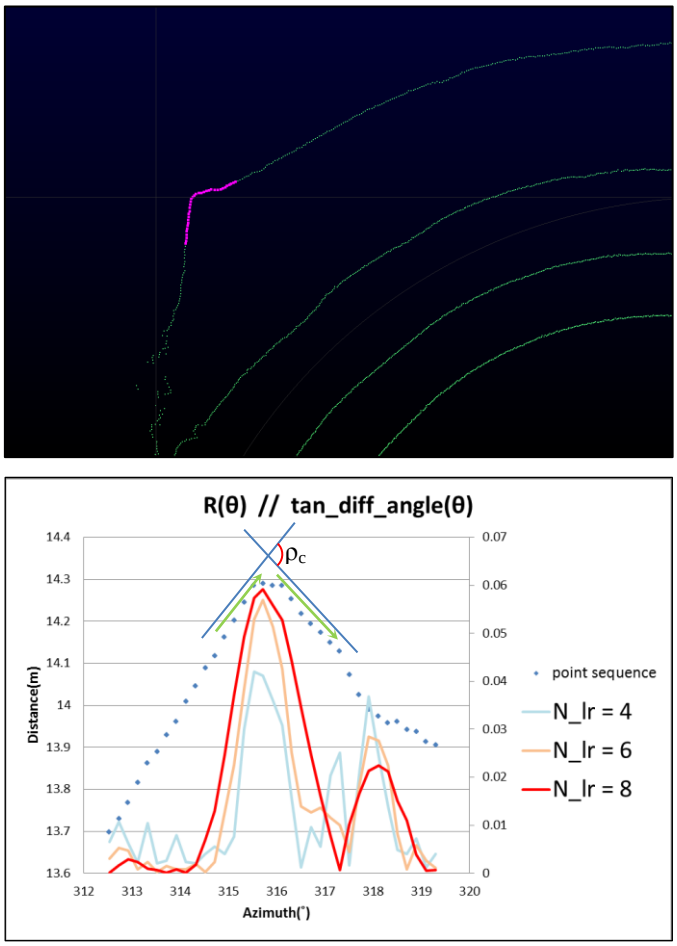

Figure 8. (top)A scan captured at regular road surface with cement curb at ≈14m. The sequence is extracted (marked in magenta) from the scan layer with φ = -9°, (bottom) the dart chart represent the R-θ distribution of all points in the extracted sequence, the line charts are the tangent value of tan ρ_c calculated with respectively N_{lr} = 4(light blue), N_{lr} = 6(orange), N_{lr} = 8(red).

I. Region growing road area recognition

As the road boundaries in each scan line have been found, it remains to generate road surface perception. We propose a region-growing method to generate the road surface expanding from a selected seed point.

First, a point is selected from the frame as the seed to begin the growing: the point is conceived to belong to the road surface itself, thus it has to be continuous, smooth, and has an elevation approximately zero as transformed by the equation (2). Since the road surface are likely to be found right in front of the vehicle, one wise choice would be selecting from the nearest scan line in front of the mounted vehicle, in VLP-16 lidar, it is the layer with φ = -15°. We could directly address to the most centered point, if it doesn't fulfill the requirement, we search left & right until it is found.

Starting from the seed point, the search on the scan line sequence are firstly executed, and is ended at both sides until either of the continuity and smoothness property is not conserved.

The sub-sequence between two extremities is built, and is called segment. From the first segment, we find the next segment by trying to get new seed at neighbor layers. From each point of the first segment, we try if its vertical neighbor in distribution order may be a good seed for the next layer. If found, we generate another segment likewise on second layer, if not, the vertical proximity search ends for this segment.

The segment has collective property, such as length, average height, slope …etc. A segment with too short length, high relative elevation, and presenting a steep slope, will be discarded from the road candidate segment set.

It should be marked that points a layer can contain multiple segment, which are for example separated by the presence of object. And a segment can have multiple neighbor segments on the same neighbor layer, as explained in Figure 9 below.

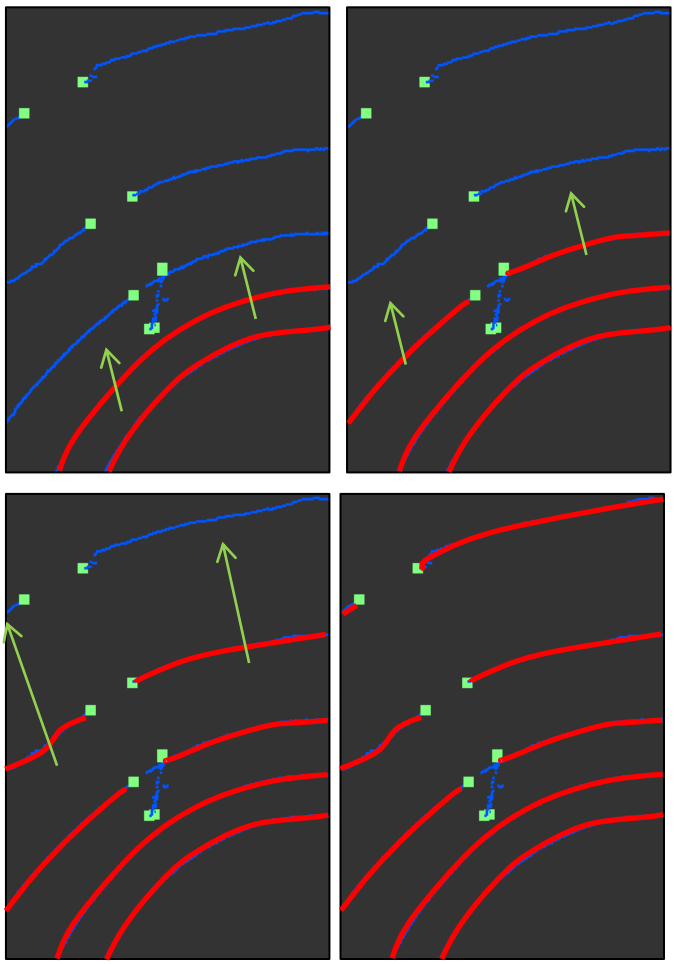

Figure 9. Region-growing algorithm with the presence of a motorcycle. The connected segments are marked in red, the discontinuous terminal points are marked in green, the continuous and smooth points in blue. The green arrow shows the neighbor search direction.

We also take into account the case where multiple un-connected road surfaces by the re-iteration seed-segment-area generation process with the points subtracted the completed connectivity search.

III. Experiment

We mount the lidar horizontally on top of an SUV as previously stated, and test our method on the output lidar scan

data. The SUV drives on the right lane of a straight double-lane road with no other vehicles or obstacles.

We evaluate the detection result on each of the 6 lowest layers of each detected frame with success / missing as shown in the Figure 10 below.

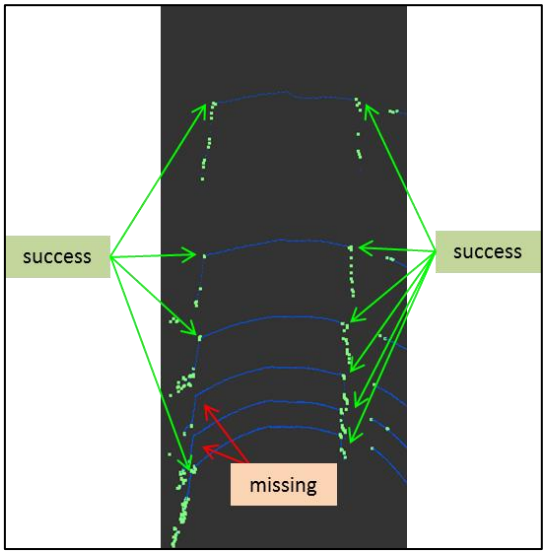

Figure 10. The scenario and evaluation method of the experiment

The evaluation was carried out through lidar output during 11.2 seconds (112frames at 10Hz), and the results are reported in the Table 1 below. We plot the statistics in the Figure 11 below to show relation between success rate, scan line average azimuth angle transition, and average edge distance.

TABLE I. EXPERIMENT EVALUATION RESULTS

Layer	layer0, φ = -15°		layer1, φ = -13°		layer2, φ = -11°		layer3, φ = -9°		layer4, φ = -7°		layer5, φ = -5°	
Side	left	Right	left	right	left	right	left	right	left	right	left	right
Azimuth angle	132°	96°	128°	97°	122°	99°	112°	104°	98°	104°	110°	105°
Distance(m)	7.27	7.51	8.47	8.70	10.19	10.32	12.70	13.00	16.56	16.88	24.00	24.62
Success rate(%)	85.7	100.0	76.8	98.2	91.1	100.0	97.3	100.0	100.0	100.0	100.0	100.0

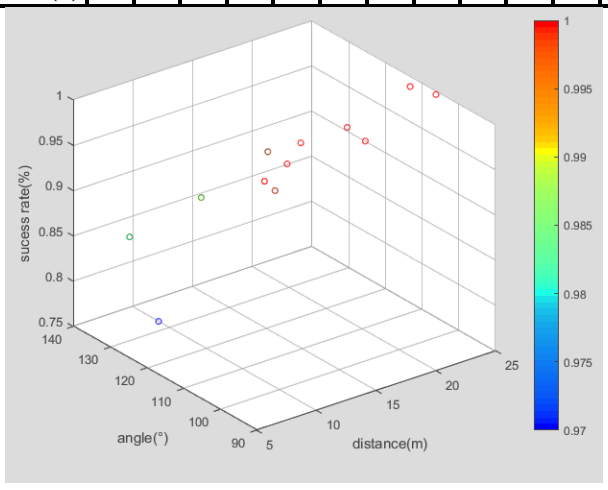

Figure 11. 3D-chart of success rate in function of edge distance and azimuth transition.

IV. CONCLUSION

A road area detection method based on 3D lidar which does not necessary requires high-resolution lidar has been built and examined by multiple test scenarios to be robust in regular road scenario. The obstacle on the road can be stably taken into account to be distinguished from the road points. However, our experiment shows that if the road side intersect with scan line with an angle > 120°, the success rate of boundary detection shows signs of decreasing.

Other types of road sides like grass or other non-rectangular road curb sometimes produces unpredicted smoothness detection missing. Limited to the resolution of lidar, although the method is still able to find the road boundary on scan lines, the detection effectiveness is attenuated in range over 30m, because the gap between layers has become so large that we are unable conclude whether the road is continue through the gap.

As next steps, we look into elaborate an adaptive filtering criterion to apply in different distance and intersection angle, in order to apply the method with higher precision and on more general scenarios.

ACKNOWLEDGMENT

This work was majorly supported by Ministry of Economic Affairs, Taiwan, under Grant 106-EC-17-A-25-1379.

.

REFERENCES

[1] R. Fernandes, C. Premebida, P. Peixoto, D. Wolf and U. Nunes, "Road Detection Using High Resolution LIDAR," 2014 IEEE Vehicle Power and Propulsion Conference (VPPC), pp.1-6, 2014.

[2] F. Moosmann, O. Pink, and C. Stiller, "Segmentation of 3D Lidar Data in non-flat Urban Environments using a Local Convexity Criterion," 2009 IEEE Intelligent Vehicles Symposium, pp. 215-220, July 2009.

[3] W. Zhang, "LIDAR-Based Road and Road-Edge Detection," 2010 IEEE Intelligent Vehicles Symposium(IV), pp.845-848, August 2010.

[4] M. Zhang, D.D. Morris and R. Fu, "Ground Segmentation based on Loopy Belief," 2015 International Conference on 3D Vision, pp.615-622, Novenber 2015.

[5] J. Byun, K. Na, B. Seo and M. Roh, "Drivable road detection with 3D Point Clouds based on the MRF for Intelligent Vehicle," Mejias L., Corke P., Roberts J. (eds) Field and Service Robotics. Springer Tracts in Advanced Robotics, vol 105., pp.49-60, 2015.

[6] X. Zhu, M. Gao and S. Li, "A real-time Road Boundary Detection Algorithm Based on Driverless Cars," 2015 4th National Conference on Electrical, Electronics and Computer Engineering, pp.843-848, January 2016.

[7] X. Yuan, C.X. Zhao and H.F. Zhang, "Road Detection and Corner Extraction Using High Definition Lidar," Information Technology Journal, vol. 9(5), pp.1022-1030, 2010.

[8] L. Caltagirone, S. Scheidegger, L. Svensson and M. Wahde, "Fast LIDAR-based Road Detection Using Fully Convolutional Neural Networks," 2017 IEEE Intelligent Vehicles Symposium (IV), pp.1019-1024, July 2017.

[9] M. Li and Q. Li, "Real-time Road Detection in 3D Point Clouds using Four Directions Scan Line Gradient Criterion," unpublished.

[10] X. Hu, S. F. Sergio A. Rodriguez and A. Gepperth, "A multi-modal system for road detection and segmentation," 2014 IEEE Intelligent Vehicles Symposium Proceedings, pp.1365-1370, July 2014.